Geomechanics and Engineering, *Vol. 16, No. 5 (2018) 471-482*
DOI: https://doi.org/10.12989/gae.2018.16.5.471

A systematic approach to the calibration of micro-parameters for the flat-jointed bonded particle model

Changtai Zhou[1], Chaoshui Xu*[1,3], Murat Karakus[1] and Jiayi Shen[2]

[1]School of Civil, Environmental and Mining Engineering, The University of Adelaide, Adelaide, Australia
[2]Institute of Port, Coastal and Offshore Engineering, Zhejiang University, Hangzhou, China
[3]School of Resource and Environmental Engineering, Wuhan University of Science and Technology, Wuhan, China

(Received November 28, 2017, Revised August 13, 2018, Accepted September 13, 2018)

Abstract. A flat-jointed bonded-particle model (BPM) has been proved to be an effective tool for simulating mechanical behaviours of intact rocks. However, the tedious and time-consuming calibration procedure imposes restrictions on its widespread application. In this study, a systematic approach is proposed for simplifying the calibration procedure. The initial relationships between the microscopic, constitutive parameters and macro-mechanical rock properties are firstly determined through dimensionless analysis. Then, sensitivity analyses and regression analyses are conducted to quantify the relationships, using results from numerical simulations. Finally, four examples are used to demonstrate the effectiveness and robustness of the proposed systematic approach for the calibration procedure of BPMs.

Keywords: discrete element method; bonded-particle model; flat-jointed model; micro-parameters; macro-rock properties; intact rocks

1. Introduction

Numerical modelling provides the possibility for understanding the complexity of rock mechanical behaviours via analogy simplification. Cundall (1971) proposed the discrete element method (DEM) to simulate the microstructure features and mechanical properties of intact rocks. The particle flow code (PFC) (Itasca Consulting Group Inc 2014), as the most widely used DEM code in geomechanics, uses a granular assembly following Newton's law of motion. Such models are based on the belief that one can replicate the macro-properties of intact rocks if one can reproduce rock's microstructures and the corresponding interactions between them.

At the early stage, PFC models were limited to simulating the mechanical behaviours of cohesionless granular materials without bonds between particles (Cundall and Strack 1979). In 2004, the bonded-particle model (BPM) (Potyondy and Cundall 2004) was introduced to reproduce the microstructures (see Fig. 1) and its corresponding macro-properties for intact rocks.

BPM can reproduce the behaviours of particle assemblies bonded by cementations, which mimic both the microstructure and the mechanical behaviours of intact rocks. The mechanical behaviours investigated in the literature include elasticity (Potyondy and Cundall 2004, Schöpfer *et al.* 2007), fracturing (Zhao *et al.* 2015, Zhou *et al.* 2016), failure processes (Duan *et al.* 2015b), damage zones (Fakhimi and Villegas 2007), rock cutting (He and Xu 2015), crack initiation and coalescence processes (Ning *et al.* 2015, Tian and Yang 2017, Vesga *et al.* 2008) and shearing behaviours of soil-rock mixture (Xu *et al.* 2015).

Three BPMs, the linear-bond model (LBM), the parallel-bond model (PBM) and the flat-jointed model (FJM), are provided in PFC (Itasca Consulting Group Inc 2014). PBMs and FJMs are the most widely used in brittle rock simulations, which can produce a good match of mechanical behaviours of rocks at lab scales. However, a BPM with a LBM or a PBM suffers from three intrinsic problems: the unrealistic ratio of uniaxial compressive strength (UCS) to tensile strength (TS), the unrealistic low internal friction angle, and the unrealistic linear failure envelope (Cho *et al.* 2007, Potyondy and Cundall 2004, Schöpfer *et al.* 2007, Wu and Xu 2016). These limitations can be addressed in two ways: By either increasing interlock in the numerical models, i.e., creating clumps of particles (Cho *et al.* 2007), which will increase computation time; or by introducing a grain-based model.

Potyondy (2012) reproduced the stress-strain behaviours of granite by using uniaxial compression tests and biaxial compression tests with the FJM. The work also revealed that macro-properties such as Young's modulus (E), Poisson's ratio (ν) and UCS can be matched to the laboratory data, and so too can the ratio of UCS to TS. Using a three-dimensional (3D) analysis, Wu and Xu (2016) confirmed that the unrealistically low ratio of UCS to TS can be fixed through FJM. They further explored the excessively low internal friction angle and the unrealistic failure envelope through uniaxial compression tests and triaxial compression tests. Vallejos *et al.* (2016) compared the PBM and FJM for intact rock simulations, and highly recommended FJM for intact rock simulations with and without confining pressures.

*Corresponding author, Professor
E-mail: chaoshui.xu@adelaide.edu.au

http://www.techno-press.org/?journal=gae&subpage=7
ISSN: 2005-307X (Print), 2092-6219 (Online)

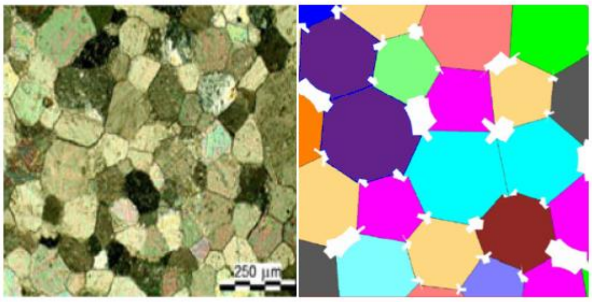

Fig. 1 The scanning electron microscopy image of marble on the left, and the flat-jointed model material on the right

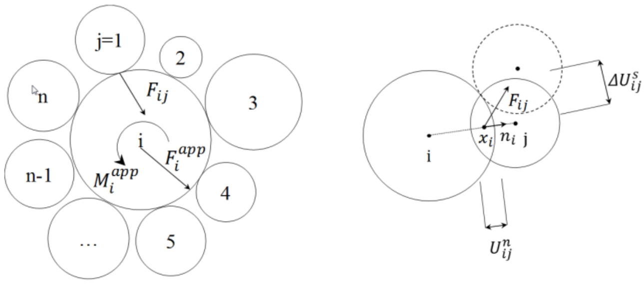

(a) (b)

Fig. 2 (a) Forces and moments acting on a particle and (b) Force-displacement behaviour at a contact

Despite the successful applications of the FJM for intact rock simulations, one issue remains unresolved: there are no direct relationships between micro-parameters of the FJM and the macro-mechanical properties of the rock being analysed. A tedious and time-consuming calibration process, on a trial and error basis, is normally required. This process involves performing numerical uniaxial compression tests, and direct or indirect tensile strength tests to derive a set of micro-parameters for the BPM using FJM. The time-consuming calibration process imposes significant restrictions on FJM's widespread applications for solving rock engineering problems. Numerous studies to address this issue for the PBM have been published (Fakhimi and Villegas 2007, Huang 1999, Yang *et al.* 2006). For example, a dimensionless analysis (Huang 1999) was introduced in the calibration procedure, which was proven to be more efficient and convenient (Fakhimi and Villegas 2007, He and Xu 2015, Yang *et al.* 2006). Yang *et al.* (2006) further proposed some empirical quantitative relationships to derive macro-properties of numerical models from micro-parameters. In contrast, for FJM, we found no published studies that quantify the relationships between micro-parameters and the macro properties of rocks. These relationships are expected to be completely different to those for the PBM because of their different mechanical behaviours at the micro-level (Potyondy 2012).

This paper aims to quantify the relationships between micro-parameters and macro-rock properties for FJM, which can then be used to build more effective and consistent numerical models for subsequent DEM studies. First, the background theory of FJM is reviewed. Using dimensionless analysis, we introduce the initial relationships between the micro-parameters and macro-properties of FJM. Then, a set of microscopic structure parameters that can generate a well-connected and isotropic particle assembly are determined. This paper then presents the results of uniaxial compression tests and direct tension tests, which are carried out to evaluate the effects of the individual, microscopic, constitutive parameters on macro-rock properties. The results are used to simplify the proposed initial relationships. Regression analyses are performed based on the dimensionless analyses and the numerical modelling results to quantify the relationships. Finally, the performance of the derived relationships is assessed by testing them against four different types of rocks.

2. Relationships between micro-parameters and macro-rock properties of FJM

In this section, the fundamentals of FJM are reviewed, and the initial relationships between micro-parameters and macro-rock properties are introduced through dimensionless analysis.

2.1 Background theory of BPM

The BPM was introduced to simulate the mechanical behaviours of an assembly of rigid particles that are bonded together at and interact with each other through their contacts. The movement of these particles follows Newton's law of motion, while the interaction between particles is determined by constitutive models implemented at their contacts. The motion of particles includes two components: translational motion and rotational motion. As shown in Fig. 2(a), contact force and moment arisen when two particles come into contact are

$$F_i = \sum_{j=1}^{n} (F_{ij}^n + F_{ij}^s) + F_i^{app} \tag{1}$$

$$M_i = \sum_{j=1}^{n} F_{ij}^s r_{ij} + M_i^{app} \tag{2}$$

where r_{ij} is the distance from centre of particle i to the contact point between particle i and particle j; F_i^{app} and M_i^{app} are the additional force and moment applied to particle i; F_{ij}^n and F_{ij}^s are the normal and shear contact forces in the local coordinate system between particle i and particle j, respectively, see Fig 2(b)

$$F_{ij}^n = k_{ij}^n U_{ij}^n \tag{3}$$

$$F_{ij}^s = -k_{ij}^s \Delta U_{ij}^s \tag{4}$$

where k_{ij}^n and k_{ij}^s are the normal and shear stiffness of the contact between particle i and particle j, U_{ij}^n is the overlap used to simulate the deformation of the particle in the normal direction, and ΔU_{ij}^s is the shear displacement increment between particle i and particle j.

To simulate the quasi-static condition in DEM using the dynamic formulation implementation discussed above, some form of damping is necessary to dissipate the kinetic energy. In this study, the global damping was applied to damp out the particle accelerations.

2.2 Basic theory of FJM

The FJM provides the macroscopic behaviour of a finite-size, linear elastic, and either bonded or frictional interface that may sustain partial damage. The interface, a flat line in 2D, or a flat disc in 3D, can be discretised into several segments or several areas respectively (elements).

A contact of FJM is active when any element is either bonded or has a negative gap. The contact may be deleted at the discretion of the contact detection logic when the distance between the notional surfaces becomes greater than the initial surface gap g_0. The implemented constitutive model of FJM is described in PFC manual (Itasca Consulting Group Inc 2014). The force-displacement relationship and yielding criterion are briefly described below.

The force-displacement relationship of FJM is determined by the relative displacement of two notional surfaces. Each of the equally discretised elements carries a force (F^e) and a moment (M^e), and can be either bonded or de-bonded at the centre of the interface, which coincides with the contact location. Then the normal stress and shear stress of FJM can be calculated.

When the bonded element is under tension, the tensile stress sustained by the bonded element can increase until the tensile strength of the bond is exceeded; then, the bonded element breaks (a tensile crack) and becomes a de-bonded element. The tensile strength of a de-bonded element by definition is zero. On the other hand, the shear strength of FJM follows the Mohr-Coulomb (MC) criterion, i.e.,

$$\tau^e = c + \sigma^e \tan\phi_b \tag{5}$$

where c is the bond cohesion and ϕ_b is the local friction angle. The bonded element will break into a shear crack when the shear strength of the bond is exceeded. On the other hand, the shear strength of a de-bonded element obeys the Coulomb sliding criterion

$$\tau^e = \sigma^e \tan\phi_r \tag{6}$$

where ϕ_r is the residual friction angle. The strength envelope of a bonded element is shown in Fig. 3.

It is worthwhile to mention that for the FJM, the interface may evolve from a fully bonded state to a fully de-bonded and frictional state. Note that the breakage is brittle in FJM. However, the fully de-bonded interface is not removed during the simulation, so the interface will continue to resist relative rotation. This fictitious notional surface can, therefore, increase the ratio of UCS to TS by grain interlocking, which reflects rock behaviours more realistically at a micro scale, and is more advantageous compared with other bonded particle models (Potyondy 2012, Wu and Xu 2016).

For elastic deformability, in the latest version of PFC (Itasca Consulting Group Inc 2014), deformability method is employed to substitute the contact model properties. In this approach, the elastic contact properties, such as k_n and k_s, are not specified directly; rather, k_n and k_s of contacts are modified in the programme simultaneously to meet a target effective modulus (E^*) of the ball assembly. More details can be found in related works (Potyondy 2012, Wu and Xu 2016) and PFC manual (Itasca Consulting Group Inc, 2014).

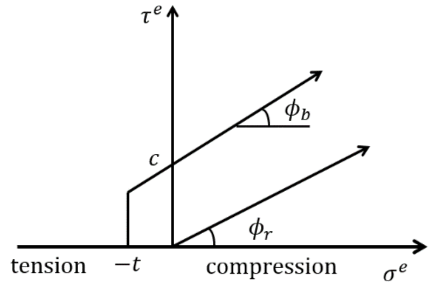

Fig. 3 Failure envelopes for bonded elements and de-bonded elements (Wu and Xu 2016)

Table 1 Three groups of micro-parameters of BPM

Groups	Micro-parameters	Symbol	Unit	Base unit
Boundary condition parameters	Specimen width	w	mm	L
	Specimen height	l	mm	L
	Loading rate	V	m/s	L·T^{-1}
Micro-structures and geometrical parameters	Ratio of maximum to minimum ball radius	r_{max}/r_{min}	[-]	[-]
	Ratio of specimen width to the median ball diameter	w/d	[-]	[-]
	Bond surface gap	g_0	m	L
	Porosity of the synthetic numerical specimen	n	[-]	[-]
	Number of elements in each bond	N_r	[-]	[-]
Micro-mechanical and constitutive parameters	Effective modulus of bond	E^*	GPa	F·L^{-2}
	Stiffness ratio of contact	k^*	[-]	[-]
	Tensile strength of contact	t	MPa	F·L^{-2}
	Cohesion of bond	c	MPa	F·L^{-2}
	Friction angle of bond	ϕ_b	°	[-]
	Residual friction coefficient of bond	μ	[-]	[-]

Note: [*F, L, T*] represent the primary dimension of force, length and time respectively

2.3 Preliminary relationships between micro-parameters and macro-properties

The dimensionless method (Fakhimi and Villegas 2007, He and Xu 2015, Huang 1999, Yang *et al.* 2006), through uniaxial compression tests and direct tension tests (Fig. 4), was proved to be useful and efficient for establishing the relationships between macro-mechanical properties and micro-parameters. The BPM parameters can be divided into three groups: boundary conditions, micro-structure and geometrical parameters, and micro-mechanical and constitutive parameters between the particles, as shown in Table 1.

The mechanical properties, such as UCS, TS, E and ν of FJM are governed by these parameters listed in Table 1. Dimensionless analysis, based on the Buckingham π theorem (Sonin, 2004), was employed to establish the initial relationships between micro-parameters and macro properties of rocks for further investigation. Simply, a physical meaningful equation $\Phi(q_1,q_2,...,q_n)=0$, where q_i is a physical variable, can be rewritten in terms of a set of dimensionless parameters $\phi(\pi_1,\pi_2,...,\pi_n)=0$, where π_i is the dimensionless variable constructed from the original variable. Therefore, different mechanical properties of FJM can be expressed in term of dimensionless parameters constructed from these micro-parameters.

In this study, the loading rate V, one of the boundary parameters, was removed from the analysis because only the quasi-static loading conditions were considered. For this reason, and based on the work done in previous studies and the PFC manual (Itasca Consulting Group Inc, 2014), V is set to 0.02 m/s. Therefore, there are a total of 10 physical parameters, $\{r_{max}/r_{min}, w/d, N_r, n, k^*, \tan\phi_b, \mu, E^*, c, t\}$ for the FJM, which can be represented by 9 dimensionless parameters: $\{r_{max}/r_{min}, w/d, N_r, n, k^*, \tan\phi_b, \mu, E^*/c, t/c\}$.

The mechanical properties, such as UCS, TS, E and ν of FJM are governed by these parameters listed in Table 1. Dimensionless analysis, based on the Buckingham π theorem (Sonin 2004), was employed to establish the initial relationships between micro-parameters and macro properties of rocks for further investigation. Simply, a physical meaningful equation $\Phi(q_1,q_2,...,q_n)=0$, where q_i is a physical variable, can be rewritten in terms of a set of dimensionless parameters $\phi(\pi_1,\pi_2,...,\pi_n)=0$, where π_i is the dimensionless variable constructed from the original variable. Therefore, different mechanical properties of FJM can be expressed in term of dimensionless parameters constructed from these micro-parameters.

In this study, the loading rate V, one of the boundary parameters, was removed from the analysis because only the quasi-static loading conditions were considered. For this reason, and based on the work done inprevious studies and the PFC manual (Itasca Consulting Group Inc 2014), V is set to 0.02 m/s. Therefore, there are a total of 10 physical parameters, $\{r_{max}/r_{min}, w/d, N_r, n, k^*, \tan\phi_b, \mu, E^*, c, t\}$ for the FJM, which can be represented by 9 dimensionless parameters: $\{r_{max}/r_{min}, w/d, N_r, n, k^*, \tan\phi_b, \mu, E^*/c, t/c\}$.

The macro elastic properties, namely E and ν, are determined by the E^* and k^* in the elastic regime where no failure occurs (Huang 1999, Potyondy and Cundall 2004). However, the macro-strength properties, such as UCS and TS in the numerical model, depend on both the bond/interface strength parameters and the micro-elastic parameters. Invoking the Buckingham π theorem, the following equations are suggested for the relationships between micro-parameters and macro-parameters (He and Xu 2015, Huang 1999)

$$\frac{E}{E^*}=f_E(k^*,n,N_r) \tag{7}$$

$$\nu=f_\nu(k^*,n,N_r) \tag{8}$$

$$\frac{\sigma_c}{c}=f_c\left(\frac{E^*}{c},k^*,\frac{t}{c},\mu,\phi_b,n,N_r\right) \tag{9}$$

$$\frac{\sigma_t}{t}=f_t\left(\frac{E^*}{c},k^*,\frac{t}{c},\mu,\phi_b,n,N_r\right) \tag{10}$$

3. Sensitivity analysis for the effects of individual parameters on the macro-properties

In this section, the influences of micro-structural parameters of the BPM on macro properties were discussed based on both previous studies and current numerical simulations in order to generate a homogenous, isotropic and well-connected granular assembly. A sensitivity analysis was then used to investigate the effects of individual constitutive micro-parameters on macro-rock properties. Parameters that have limited or no effects on the corresponding macro-properties were removed from the relationship. As shown in Fig. 4, a rectangular specimen of 54×108 mm, with randomly distributed particles, was used to perform uniaxial compression tests and direct tension tests for sensitivity analysis.

3.1 Micro-structural parameters of the BPM

3.1.1 The number of elements (N_r)

Discrete bond elements are first introduced in FJM so their effects on macro rock properties need to be investigated. In this study, we progressively increased the number of elements for each interface from 1 to 6 to examine their impacts on stress-strain curves of the specimen and the results are shown in Fig. 5, which indicates that the number of elements has limited effect on the mechanical properties of FJM.

The mechancial properties and their corresponding coefficients of variation (COV) are listed in Table 2. The results show that the number of elements for each interface has no effect on the tensile strength while it has a very limited effect on the UCS, E and ν with COV less than 2%. Therefore, this variable was removed from further investigations in this study.

3.1.2 Ratio of maximum to minimum ball radius (r_{max}/r_{min})

The r_{max}/r_{min} ratio is related to the particle size distribution, and there are mixed conclusions on its influence on the corresponding macro-properties. Ding *et al.* (2014) indicated that UCS and E increase while the ν shows an opposite trend with an increasing r_{max}/r_{min} ratio. Yang *et al.* (2006), however, pointed out that no obvious effects on E, ν and UCS can be found based on simulation results. Koyama and Jing (2007) argued that the particle size distribution has very limited effects on the macro-properties (E, ν, UCS and TS) when the ratio of specimen width to the median ball radius w/d exceeds a threshold value. Huang (1999) suggested that the particle ratio can be removed from consideration when a particle assembly has a

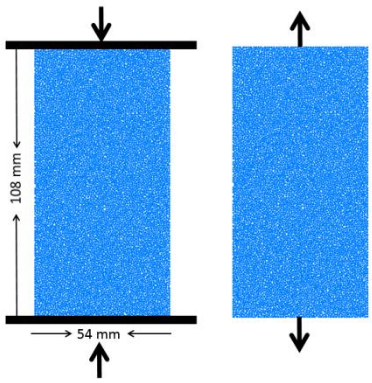

Fig. 4 Bonded-particle models for the uniaxial compressive test (left) and direct tension test (right)

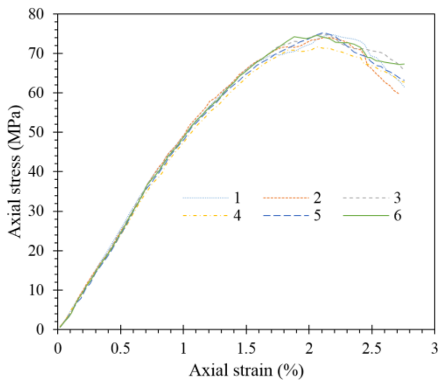

Fig. 5 Stress-strain curves with different numbers of elements for each bond

Table 2 Macro-properties of FJM with different number of elements for each bond and the corresponding COV

Numbers of element	UCS (MPa)	TS (MPa)	E (GPa)	v
1	75.18	2.03	5.31	0.161
2	74.23	2.03	5.30	0.161
3	75.13	2.03	5.29	0.161
4	72.01	2.03	5.14	0.159
5	75.63	2.03	5.32	0.161
6	74.89	2.03	5.31	0.161
COV (%)	1.76	0.00	1.29	0.51

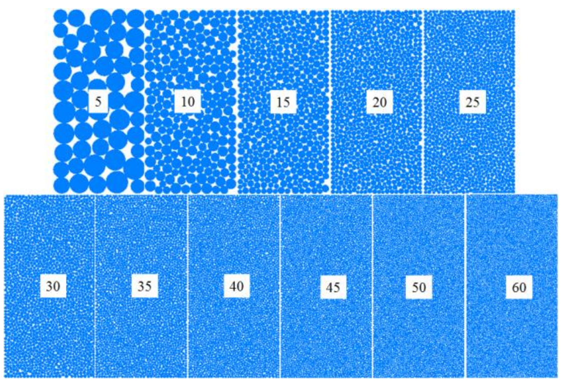

Fig. 6 The schematic view of a stochastic procedure for BPM model generation. The *w/d* ratio varying from 5 to 60 to create 11 models, with 10 realisations generated for each configuration.

sufficient degree of freedom. Previous investigations (Huang 1999, Koyama and Jing 2007, Yang *et al.* 2006) show that the r_{max}/r_{min} ratio of published researches falls in the range of 1.32-3.00; and 1.66 is the most common choice for the simulation of brittle rocks. Therefore, to simplify the BPM establishment process, we suggested that the r_{max}/r_{min} ratio is set at 1.66 so it is removed from further considerations.

3.1.3 Porosity (n)

The porosity (n), related to the damage in rock (Xue 2015), in PFC-2D is the ratio of the total void area within the specimen to the total area of the specimen, which is in general higher than that of natural rock material. This is because PFC models use circular particles to represent rock grains, which is a major limitation of PFC implementation. Porosity n is a good index for representing particle distribution parameters that are related to the coordination number, defined as the number of contacts per particle. The relationship between the porosity and the coordination numbers was established by Oda *et al.* (1982). Many studies (Ding *et al.* 2014, Schöpfer *et al.* 2007, Yang *et al.* 2006) indicate that UCS, TS and E decrease with increasing n, while the ν is not affected. On the other hand, computational efficiency can be substantially increased as n increases (Wang *et al.* 2014, Yang *et al.* 2006) because of the reduction in the numbers of particles.

In this study, to simplify the process, n was removed from further considerations by setting n to the constant value of 0.16, which corresponds to the porosity when the most commonly used r_{max}/r_{min} ratio of 1.66 is used according to previous studies (Potyondy 2012, Potyondy and Cundall 2004, Yoon 2007).

3.1.4 Ratio of specimen width to the median ball diameter (w/d)

As mentioned earlier, the *w/d* ratio influences the macro-mechanical properties of intact rocks. For FJM, a proper ratio needs to be found for numerical simulations. This ratio also implicitly defines the size of particles that have to be used, given a specific specimen scale. Previous studies covered a wide range of the *w/d* ratio for other bond models, from 5 to 200 (Huang 1999, Potyondy and Cundall 2004). These results indicate that the elastic properties and strength properties suffer large variations when the *w/d* ratio is low, and they converge to a constant value when this ratio is greater than 50 (Koyama and Jing 2007).

To find a suitable value for FJM, we progressively increased the *w/d* ratio from 5 to 60, with 10 stochastic realisations for each ratio to create 11 different numerical models, as shown in Fig. 6. In the stochastic realisations, the geometrical properties such as initial position and size are randomly attributed to particles according to different random seeds.

Fig. 7 shows the scatter plot and mean values of UCS, E and ν versus the *w/d* ratio. The coefficient of variation (COV) is used to evaluate the variability of the macro-properties for different *w/d* ratios and is also plotted in Fig. 7. The results show that the average UCS and ν decrease while the E increases as the *w/d* ratio increases, which is consistent with the results by Koyama and Jing (2007),

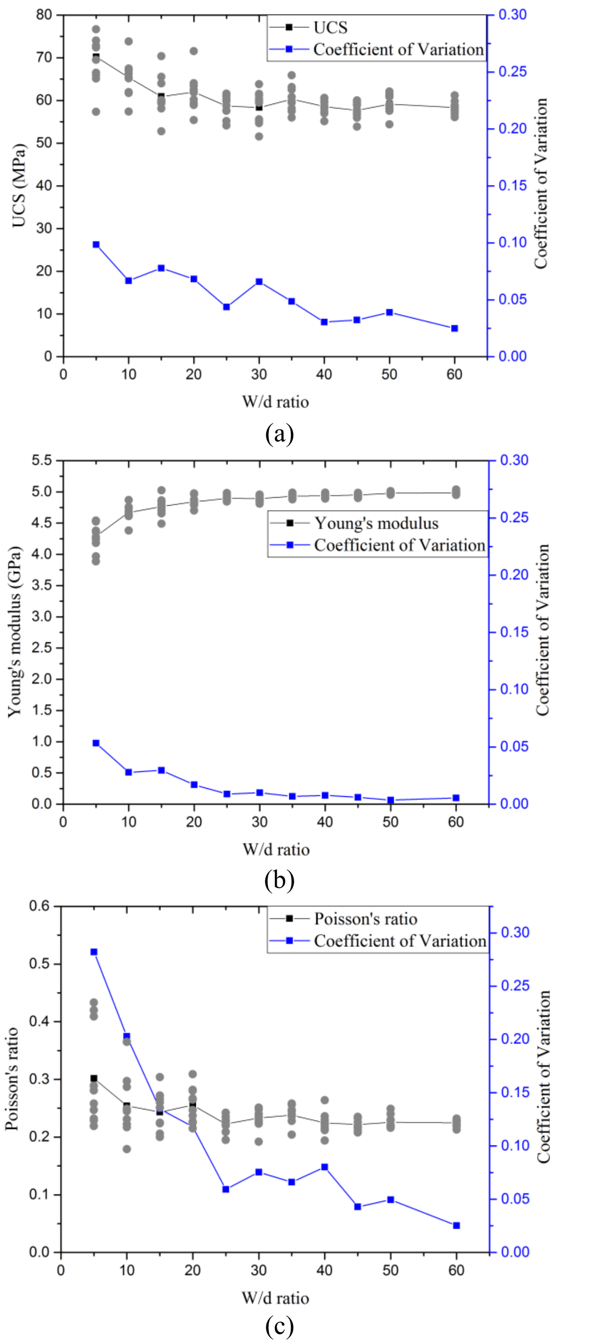

Fig. 7 Variations of macro-properties for different w/d ratios, with 10 realizations for each ratio, (a) UCS, (b) E and (c) ν

Table 3 Boundary and micro-structure parameters for the FJM

Boundary parameters			Microstructure parameters				
w (mm)	l (mm)	V (m/s)	r_{max}/r_{min}	g_0	N_r	n	w/d
54	108	0.02	1.66	1e-4	3	0.16	45

Schöpfer *et al.* (2007) and Yoon (2007).

The acceptable COV used to determine a suitable w/d ratio was set to 5%. The simulation results show that the optimal ratios are 40 and 45 in terms of UCS and ν, but it is found to be 10 for E because of its low variability with different w/d ratios. Therefore, a minimum w/d ratio of 45 was selected, which ensures that macro-properties such as UCS, E and ν converged to a stable value.

To summarize, the final boundary parameters and micro-structural parameters for the FJM that were suitable for simulating the mechanical behaviours of rock materials are summarised in Table 3.

The determination of these micro-structural parameters is a prerequisite for generating a suitable and consistent homogenous and isotropic particle assembly, for both laboratory-scale investigation and large-scale field application problems. Each numerical model should have enough number of particles to ensure that the model has a large sufficient degree of freedom so that stable and reliable mechanical behaviours can be obtained. At the micro-scale, each particle should have at least three contacts to ensure that the particle in the model is stable and well-connected so that flat-jointed bonds can be properly installed. These contacts are largely influenced by the initial gap g_0 and porosity n. If the micro-structure parameters listed in Table 3 are used, the average contact number is 4.08, indicating a well-connected BPM.

Table 4 Initial constitutive parameters for sensitivity analysis

k^*	E^*	t	c	ϕ_b
2	20 (GPa)	4 (MPa)	40 (MPa)	35 (°)

Table 5 COV of macro-properties corresponding to individual parameters

COV (%)	E	ν	σ_c	σ_t
Stiffness ratio, k^*	5.49	22.38	2.89	2.43
Effective modulus, E^*	62.96	0.35	1.85	0.58
Bond tensile strength, t	0.25	0.38	0.14	18.64
Bond Cohesion, c	0.12	0.24	28.59	0.00
Local Friction angle, ϕ_b	0.14	0.32	69.50	0.00

3.2 Constitutive parameters

In this section, influences of individual constitutive parameters of FJM on macro-properties such as UCS, TS, E and ν are investigated through sensitivity analysis. The initial microscopic constitutive parameters for sensitivity analysis are listed in Table 4. The results are summarised in Fig. 8. The macro-properties are normalised by the maximum value of the corresponding macro-properties. Table 5 lists the variability of macro-properties for different ranges of constitutive micro-parameters, expressed in the form of coefficient of variation (COV). Detailed discussions of these results are given below.

3.2.1 Stiffness ratio (k)*

The effects of k^* on the macro-elastic and strength properties of the synthetic rock, when k^* increases from 1.4 to 3.6, are illustrated in Fig. 8(a). Obviously, the influences on both E and ν are significant. As k^* increases, the E of BPM material decreases, but the ν increases. These results

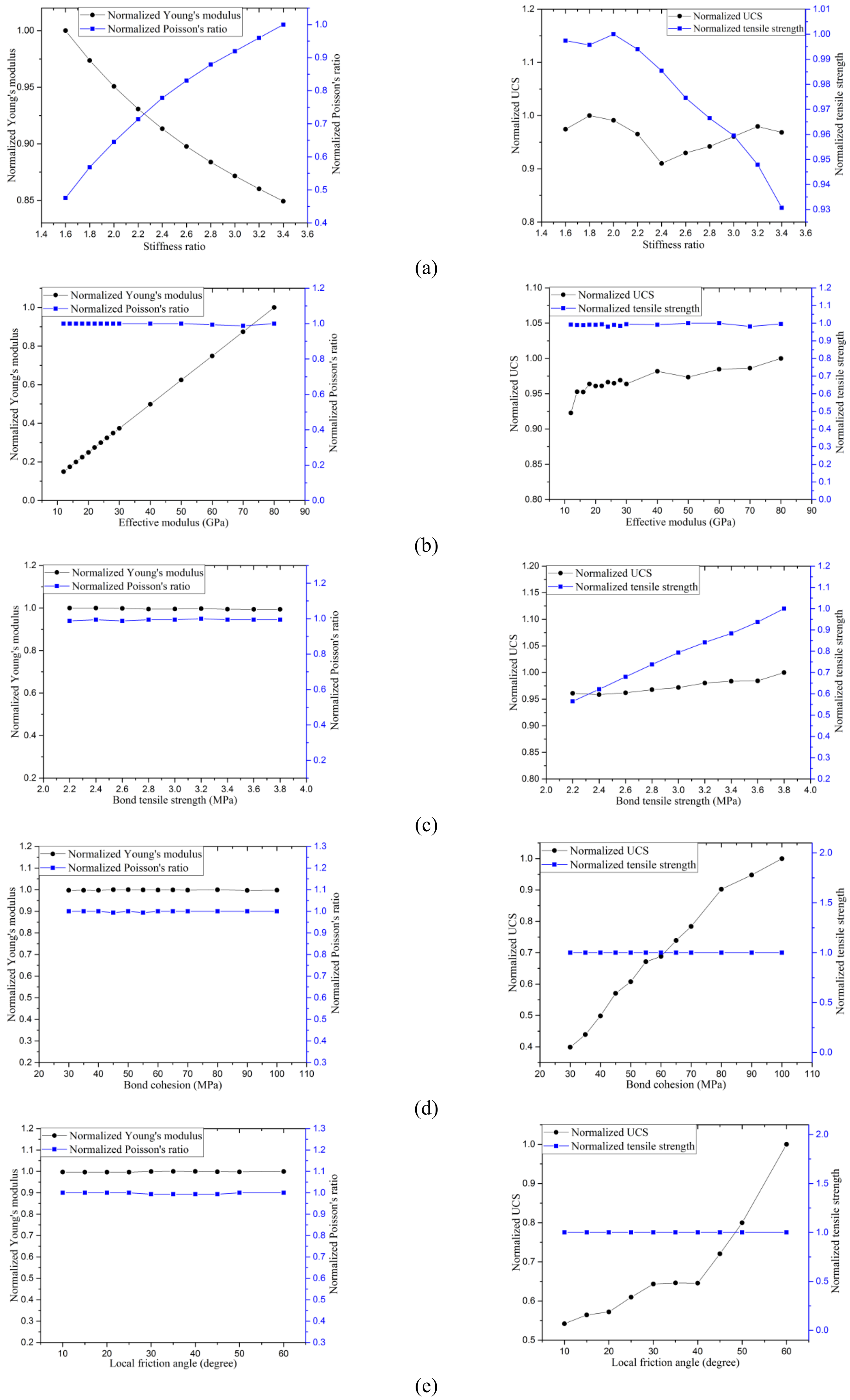

Fig. 8 Macro-properties of FJM with variation of individual parameters: (a) stiffness ratio, (b) effective modulus, (c) bond tensile strength, (d) bond cohesion and (e) internal friction angle

for the FJM are consistent with previous works with PBM (Fakhimi and Villegas 2007, He and Xu 2015, Huang 1999, Yang *et al.* 2006). Therefore, k^* is the dominant factor for calibrating these two macro-elastic properties with the COV of 5.49% and 22.38% respectively, indicating significant variations.

On the other hand, k^* has a limited effect on UCS and TS, with a COV value of only 2.89% and 2.43%, respectively. Slight decreases in UCS and TS can be seen as k^* increases. However, the tendency for the variation of UCS is not clear, and the benefit of including k^* in the determination of UCS should be further assessed.

3.2.2 Effective modulus (E*)

Young's modulus E is linearly dependent on the E^* for the FJM material (see Fig. 8(b)). The relationship is dominant with a COV of 62.96%, much higher than the COV by other micro-parameters, including k^* discussed above. The influence of E^* on v and TS can be ignored where the corresponding COV is less than 1%. UCS increases slightly when E^* increases, but the corresponding COV value is relatively low at 1.85%.

3.2.3 Bond tensile strength (t)

Elastic properties are found to be independent of t of the FJM, as shown in Fig. 8(c). These results are consistent with that for PBM. As expected, for the strength properties of BPMs, this parameter dominates the influence on the TS with a linear relationship and a COV value of 18.64%. On the other hand, the UCS increases with increasing t, as local tensile failure causes damages and therefore contributes globally to the strength reduction. As the trend of variation is clear, t was also included in the relationship to determine the UCS of the FJM.

3.2.4 Bond cohesion (c)

The simulation results reveal that the elastic properties (E and v) are independent of c with COV of only 0.12% and 0.24% respectively, see Fig. 8(d). This is consistent with previous investigations using PBM. For macro-strength properties, the TS is independent of c and therefore c can be excluded from the function to estimate the TS of FJM material. On the other hand, the UCS of FJM material has a positive linear relationship with c, one of the primary factors governing the UCS, with a COV of 28.59%. It is strange at the first sight that c has effect on UCS but not on TS. This phenomenon, however, lies in the fact that tensile failure and shear failure are governed by two separate parameters t and c at the particle level due to DEM implementation, as mentioned in Section 2.1.

3.2.5 Local friction angle (ϕ_b)

Finally, the ϕ_b was studied to assess its influences on the macro-properties of FJM (see Fig. 8(e)). As the residual friction angle ϕ_r (Fig. 3) only influences the post-peak behaviours (beyond the scope of the current study), but has no effect on the pre-failure macro-properties based on previous study (Wu and Xu 2016), this parameter is not included further in this study. Fig. 8(e) suggests that ϕ_b has no effect on the E and v, because ϕ_b will not take any effect until the bond breaks and sliding between particles occurs. For the same reason, the ϕ_b also has no effect on the TS and therefore can be removed from of the relationship for TS. However, the resistance to sliding between particles has the dominant effect on the UCS of FJM with a COV of 69.50%. This is perhaps one of the merits of FJM as resistance to sliding between rock grains at the micro-scale under compression is the behaviour expected from rock materials.

Based on the results discussed above for FJM materials, E is affected by $E^*$and k^* but v is only related to k^*. For strength properties, TS is determined by k^* and t, while UCS has a more complex relationship with almost all constitutive micro-parameters. Therefore, the initial relationships are modified to give more practical functions below

$$\frac{E}{E^*}=f_E(k^*) \tag{11}$$

$$v=f_v(k^*) \tag{12}$$

$$\frac{\sigma_c}{c}=f_c\left(\frac{E^*}{c},k^*,\frac{t}{c},\mu,\phi_b\right) \tag{13}$$

$$\frac{\sigma_t}{t}=f_t(k^*) \tag{14}$$

When employing the Mohr-Coulomb (MC) failure criterion and the deformability method discussed above at the particle level, FJM can reproduce realistic macro-mechanical properties of intact rocks. The deformability properties, such as E and v, are elastic properties before failure and only relate to microscopic deformability parameters such as E^* and k^*. However, the macro-strength properties, UCS and TS, are dependent at the particle level not only on the micro-strength parameters but also the micro-deformability parameters. A possible explanation for this is that the elastic mismatch at the particle level will induce stress related localised tensile failure, which may evolve into shear failure at the global scale.

4. Regression analysis

The simplified relationships listed above can be further quantified using regression analysis based on numerical simulation results. We used linear regression, non-linear regression and multivariate regression techniques to obtain the best-fit relationships for different macro-properties. This section presents these relationships in the order of complexity. The determination of v is the simplest, because it only depends on k^* as discussed above. Then, the relationships for E and TS are described, because they depend on two micro-parameters: E^* and k^*, t and k^*, respectively. The last relationship described is for UCS as it depends on all micro-parameters. This order of relationships should also be followed in practice to derive micro-parameters for FJM in order to match a set of given macro-rock properties. The macro-mechanical properties of BPM are derived from stress-strain curves: E and v can be obtained in the elastic region and UCS and TS can be derived at the peak of stress-strain curves under uniaxial compression tests and direct tension tests, respectively.

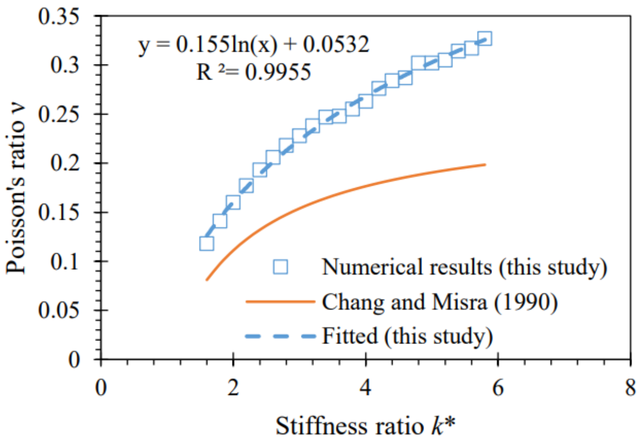

Fig. 9 Effect of k^* on Poisson's ratio and a comparison with existing analytical solution

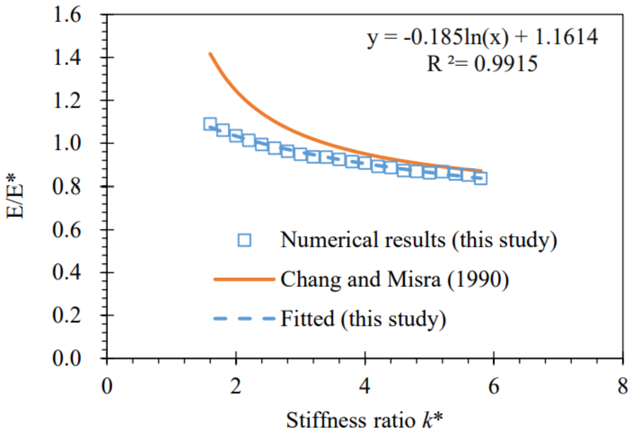

Fig. 10 Effects of k^* on the ratio of Young's modulus to the effective modulus and a comparison with existing analytical solution

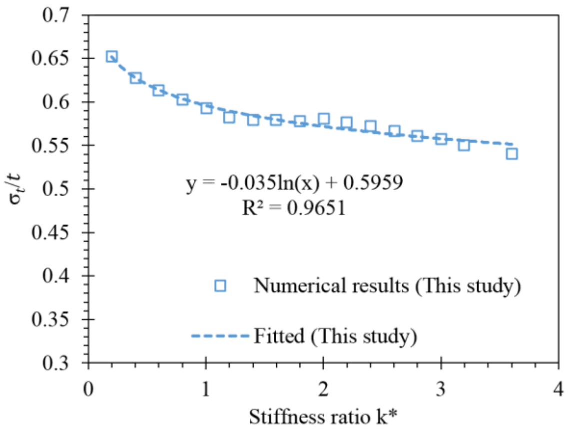

Fig. 11 Effects of k^* on the ratio of tensile strength to effective tensile strength

4.1 Poisson's ratio

Based on the sensitivity analysis conducted, Poisson's ratio ν of FJM materials is mainly determined by k^*. In this study, the range of ν covered by our numerical simulations was between 0.10 and 0.35 as shown in Fig. 9, which is the value range for most rock materials (Alejandro 2013). The best, non-linear regression gives the following expression

$$\nu=0.155\, ln(k^*) +0.053,\ R^2=0.995 \tag{15}$$

A closed-form expression for ν can be derived using a microstructure continuum approach (Bathurst and Rothenburg 1992, Chang and Misra 1990). The expression, as derived in Chang and Misra (1990) is

$$\nu=\frac{k^*-1}{4k^*+1} \tag{16}$$

This relationship is also plotted in Fig. 9 as a comparison. This analytical solution suggests that ν has a non-linear relationship with k^*. However, this closed-form solution gives an upper limit of 0.25 for ν, which is inconsistent with laboratory data. Based on our proposed relationship, k^* for FJM should be less than 20 so a realistic ν can be obtained.

4.2 Young's modulus

Young's modulus was determined by E^* and k^* of the FJM, see Eq. 11. The numerical simulation results shown in Fig. 10 suggest that a ratio of E to E^* has a non-linear relationship with the k^*. The best-fit relationship is

$$E = E^*[-0.185\ln(k^*) + 1.151], R^2 = 0.991 \tag{17}$$

An analytical solution for E was also derived in Chang and Misra (1990)

$$E=\frac{2r^2NK_n}{3V}\left(\frac{2k^*+3}{4k^*+1}\right) \tag{18}$$

where r is the radius of the particle, N is the number of contacts, K_n is the normal stiffness of contact and V is the volume of packing. The expression obtained by non-linear regression analysis is similar to the closed-form analytical equation (Eq. (18)).

As a comparison, the analytical solution is also plotted in Fig. 10. An obvious discrepancy can be seen when k^* is less than 3, but the difference gradually disappears when k^* is greater than 3.

4.3 Tensile strength

Unlike elasticity properties, no closed-form solutions can be found to link strength properties such as UCS and TS to micro-parameters of BPM. Using dimensionless analysis and numerical simulation results, the relationship between the ratio σ_t/t and k^* can be established by non-linear regression, see Fig. 11. The expression is

$$\sigma_t=t[-0.035\, ln(k^*) +0.596],\ R^2=0.965 \tag{19}$$

4.4 Uniaxial compressive strength

The UCS of FJMs demonstrates a complex, multivariate relationship with the whole set of micro-constitutive parameters, including c, t and ϕ_b, E^* and k^*. Based on the dimensionless analysis, the multivariate regression of the simulation results gives the following relationship between UCS and the micro-parameters mentioned above. The relationship is determined through regression analysis of 85 sets of micro-constitutive parameters used for uniaxial compressive tests, as shown below

$$\frac{\sigma_c}{c} = -0.056k^* + 0.777tan\phi_b + 0.1419\frac{E^*}{c} + 2.126\frac{t}{c} + 1.167, \quad (20)$$

4.5 Calibration procedure

The obtained relationships described above can be used to estimate the micro-constitutive parameters needed for applying the FJM for geomechanical analysis. In this study, the local friction angle ϕ_b was first arbitrarily determined, as it is only related to post-peak behaviours (Vallejos *et al.* 2016, Wu and Xu 2016). The following procedure should be used to derive a set of suitable micro-mechanical parameters for the FJM in order to match a set of macro-rock properties, in addition to the geometrical parameters listed in Table 3:

1. Estimate the stiffness ratio k^* through Eq. 15 to match Poisson's ratio v;
2. Estimate the effective modulus E^* through Eq. 17, with the stiffness ratio k^* determined in step 1 to match Young's modulus E;
3. Estimate the bond tensile strength t through Eq. 19, with the stiffness ratio k^* determined in step 1 to match tensile strength;
4. Estimate the bond cohesion c through Eq. 20 with stiffness ratio k^* determined in step 1, effective modulus E^* in step 2, bond tensile strength t in step 3, and pre-determined local friction angle ϕ_b to match UCS.

The proposed UCS model has a complex, multivariate relationship with micro-parameters and therefore great care should be taken to ensure if the desired UCS value can be achieved after all micro-parameters are obtained. If it is necessary to adjust the value of UCS, c can be altered until the desired UCS value is obtained as this will not affect other micro- or macro-properties because c only appears in the relationship for UCS.

5. Validation

In order to evaluate the effectiveness of the proposed empirical relationships in constructing a FJM, four different types of rocks, with different combinations of strength and elasticity properties, were used. The macro-properties of these rocks are listed in Table 6. The procedure proposed in Section 4 was employed to obtain the micro-constitutive parameters for the selected rocks, as listed in Table 7.

Numerical simulations were then performed to obtain the macro-mechanical parameters of the numerical models constructed using these micro-parameters. The numerical results are listed in Table 6 for comparison. The coefficient of variation (COV) in this case is used to quantify the discrepancy between the numerical results and the experimental data. The results show that the values of E, v and TS can be reproduced very well with COV less than 2%. The value of UCS, on the other hand, has a higher COV, ranging from 1.0% to 10.7%. This suggests greater difficulty in reproducing the UCS accurately, which is expected because of its complex relationships with almost all micro-parameters. However, the c in this case can be adjusted further to reduce the COV value for the UCS if desired.

Table 6 The comparison between experimental data and numerical simulation results of macroscopic mechanical properties of four types of rocks

Rock types		UCS (MPa)	TS (MPa)	E (GPa)	v
Avro granite[1]	Experiment	192.00	13.00	72.00	0.200
	Numerical	188.53	13.05	72.23	0.204
	COV (%)	1.289	0.271	0.225	1.400
Sandstone[2]	Experiment	107.50	11.30	35.40	0.252
	Numerical	92.39	11.36	35.42	0.255
	COV (%)	10.690	0.374	0.039	0.836
Transjurane sandstone[2]	Experiment	40.00	2.80	12.50	0.300
	Numerical	38.04	2.80	12.59	0.295
	COV (%)	3.550	0.000	0.507	1.188
Coal[2]	Experiment	22.30	0.88	18.48	0.303
	Numerical	22.62	0.927	18.71	0.287
	COV (%)	1.007	3.678	0.874	3.835
	R^2	0.9925	0.9999	0.9999	0.9832
	AAREP	6.190%	1.495%	0.579%	2.062%

[1]Olofsson and Fredriksson (2005)

[2]Peng and Zhang (2007)

Table 7 Summary of micro constitutive parameters used for the rocks studied

Rock types	k^*	E^* (GPa)	T (MPa)	c (MPa)	ϕ_b (degree)
A-granite	2.582	73.774	23.102	84.530	35.000
Sandstone	3.610	38.734	20.509	38.710	35.000
T-sandstone	4.919	14.591	5.184	18.740	35.000
Coal	5.015	21.662	1.631	11.010	35.000

A-granite: Avro granite; T-sandstone: Transjurane sandstone

For example, in order to better match the value of UCS for the sandstone, c was gradually increased until the desired UCS value was obtained. In this case, the c was increased to 45 MPa while keeping the other constitutive parameters unchanged. This caused the UCS value of the sandstone to increase from 92.39 to 106.29 MPa, with a COV value of only 0.800%. The updated micro-parameters are also listed in Table 6.

To investigate the reliability of the proposed method, the predicted macro-properties of rocks, based on numerical simulations, were compared with the experimental data in more detail. In this process, the regression R-squared value (R^2) and the average absolute relative percentage error (AAREP) were used as a measurement of discrepancy for the assessment (Shen *et al.* 2014)

$$R^2 = 1 - \frac{\sum_{i=1}^{N}(M_{R,i}^{obs} - M_{R,i}^{pred})^2}{\sum_{i=1}^{N}(M_{R,i}^{obs} - M_{R,i}^{av})^2} \quad (21)$$

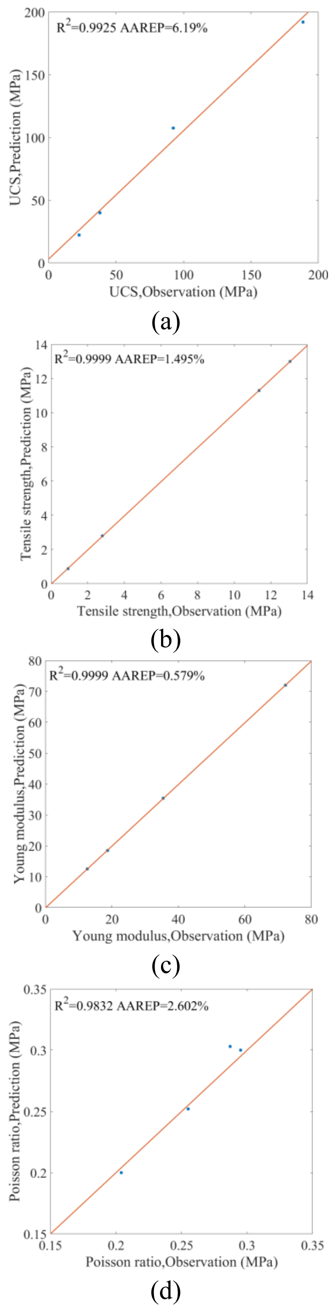

Fig. 12 Prediction performances for different macro-properties

Table 8 The comparison between experimental data and numerical simulation results of the macro-mechanical properties of Hawkesbury sandstone, with *w*/*d*=67.5

Rock type		UCS (MPa)	TS (MPa)	E (GPa)	v
Hawkesbury sandstone	Experiment	50.8	4	11	0.2
	Numerical	58.60	4.08	11.14	0.194
	COV (%)	10.08	1.40	0.89	2.15

$$\mathrm{AAREP} = \frac{\sum_{i=1}^{N}\left|\frac{M_{R,i}^{pre} - M_{R,i}^{obs}}{M_{R,i}^{obs}}\right|}{N} \tag{22}$$

where N is the total number of numerical simulations, $M_{R,i}^{obs}$ and $M_{R,i}^{pred}$ are experimental value and numerical value, respectively, and $M_{R,i}^{av}$ is the average of the numerically determined values.

The values of these discrepancy measurements are listed in Table 6. A visual comparison between experimental data and simulation results of four macro-properties is given in Fig. 12. A close agreement was observed between the data and the numerical results. The values of R^2 for all macro-properties were higher than 0.98, and the values of AAREP were less than 3%, excepting UCS, for which AAREP=6.19%.

Finally, to test the applicability of the derived relationships for different values of *w*/*d* ratio, the most important micro-structure parameter (Table 3), numerical models with *w*/*d*=67.5 are used to calibrate the macro-properties of Hawkesbury sandstone. The numerical results based on the proposed method are listed in Table 8 together with the measured properties. The COV values of TS, E and v are all below 3%, which is considered an acceptable level of discrepancy. The COV value of UCS is high initially at 10.08%. However, as discussed above, the value of c in this case can be adjusted further to reduce the COV value for the UCS if desired.

6. Conclusions

When using flat-jointed BPMs, one may encounter tedious and time-consuming calibration procedures to find a suitable set of parameters that can be used to generate a proper numerical specimen for geomechnical investigations of intact rocks if a trial and error approach is used. In order to solve this problem, a systematic approach to simplify the calibration procedure is proposed. Based on dimensionless analysis, sensitivity analysis, regression analysis and numerical simulation results, four relationships between macro-rock properties such as UCS, TS, E and v, and micro–parameters of the flat-jointed BPM such as k^*, E^*, t, c and ϕ_b were derived to facilitate the proposed parameter derivation procedure.

When determining the micro-parameters for the flat-jointed BPM, after the structural parameters (such as N_r, n, r_{max}/r_{min} and w/d) are determined, k^* should be determined based on the desired v first. E^* should then be determined to match E of the rock material, followed by t based on the TS of the rock material. Finally, the c should be determined to match the desired UCS.

The effectiveness and robustness of this approach were confirmed by the close agreement between the numerical results and the experimental results including both pre-peak and post-peak stages. Note that some additional minor adjustments of c may be necessary to achieve a better match for the derived UCS, as demonstrated in the validation test for the sandstone example.

Acknowledgements

Scholarship support for the first author provided by China Scholarship Council (CSC) is gratefully acknowledged. The authors would like to thank Leticia Mooney for her editorial support during preparation of this paper.

References

Alejandro, J. (2013), "Considerations for discrete element modeling of rock cutting", Ph.D. Thesis, University of Pittsburgh, Pittsburgh, Pennsylvania, U.S.A.

Bathurst, R.J. and Rothenburg, L. (1992), "Investigation of micromechanical features of idealized granular assemblies using DEM", *Eng. Comput.*, **9**(2), 199-210.

Chang, C.S. and Misra, A. (1990), "Packing structure and mechanical properties of granulates", *J. Eng. Mech.*, **116**(5), 1077-1093.

Cho, N., Martin, C.D. and Sego, D.C. (2007), "A clumped particle model for rock", *Int. J. Rock Mech. Min. Sci.*, **44**(7), 997-1010.

Cundall, P.A. (1971), "A computer model for simulating progressive, large-scale movements in blocky rock systems", *Proceedings of the International Symposium on Rock Mechanics*, Nancy, France, October.

Cundall, P.A. and Strack, O.D.L. (1979), "A discrete numerical model for granular assemblies", *Géotechnique*, **29**(1), 47-65.

Ding, X., Zhang, L., Zhu, H. and Zhang, Q. (2014), "Effect of model scale and particle size distribution on PFC3D simulation results", *Rock Mech. Rock Eng.*, **47**(6), 2139-2156.

Duan, K., Kwok, C.Y. and Tham, L.G. (2015), "Micromechanical analysis of the failure process of brittle rock", *Int. J. Numer. Anal. Meth. Geomech.*, **39**(6), 618-634.

Fakhimi, A. and Villegas, T. (2007), "Application of dimensional analysis in calibration of a discrete element model for rock deformation and fracture", *Rock Mech. Rock Eng.*, **40**(2), 193-211.

He, X. and Xu, C. (2015), "Discrete element modelling of rock cutting: From ductile to brittle transition", *Int. J. Numer. Anal. Meth. Geomech.*, **39**(12), 1331-1351.

Huang, H. (1999), *Discrete Element Modeling of Tool-Rock Interaction*, The University of Minnesota, Minneapolis, Minnesota, U.S.A.

Itasca Consulting Group Inc. (2014), *PFC2D/3D (Particle Flow Code in 2/3 Dimensions), Version 5.0*, Minneapolis, Minnesota, U.S.A.

Koyama, T. and Jing, L. (2007), "Effects of model scale and particle size on micro-mechanical properties and failure processes of rocks-A particle mechanics approach", *Eng. Anal. Boundary Elements*, **31**(5), 458-472.

Ning, J., Liu, X., Tan, Y., Wang, J. and Tian, C. (2015), "Relationship of box counting of fractured rock mass with hoek-brown parameters using particle flow simulation", *Geomech. Eng.*, **9**(5), 619-629.

Olofsson, I. and Fredriksson, A. (2005), *Strategy for a numerical Rock Mechanics Site Descriptive Model. Further Development of the Theoretical/Numerical Approach* (No. SKB-R--05-43), Swedish Nuclear Fuel and Waste Management Co.

Peng, S. and Zhang, J. (2007), *Engineering Geology for Underground Rocks*, Springer Science & Business Media, 1-19.

Potyondy, D.O. (2012), "A flat-jointed bonded-particle material for hard rock", *Proceedings of the 46th US Rock Mechanics/Geomechanics Symposium*, Chicago, Illinois, U.S.A., June.

Potyondy, D.O. and Cundall, P.A. (2004), "A bonded-particle model for rock", *Int. J. Rock Mech. Min Sci.*, **41**(8), 1329-1364.

Schöpfer, M.P.J., Childs, C. and Walsh, J.J. (2007), "Two-dimensional distinct element modeling of the structure and growth of normal faults in multilayer sequences: 1. Model calibration, boundary conditions, and selected results", *J. Geophys. Res.*, **112** (B10).

Shen, J., Jimenez, R., Karakus, M. and Xu, C. (2014), "A simplified failure criterion for intact rocks based on rock type and uniaxial compressive strength", *Rock Mech. Rock Eng.*, **47**(2), 357-369.

Sonin, A.A. (2004), "A generalization of the Pi-theorem and dimensional analysis", *Proc. Nat. Acad. Sci. U.S.A.*, **101**(23), 8525-8526.

Tian, W.L. and Yang, S.Q. (2017), "Experimental and numerical study on the fracture coalescence behavior of rock-like materials containing two non-coplanar filled fissures under uniaxial compression", *Geomech. Eng.*, **12**(3), 541-560.

Vallejos, J.A., Salinas, J.M., Delonca, A. and Mas Ivars, D. (2016), "Calibration and verification of two bonded-particle models for simulation of intact rock behavior", *Int. J. Geomech*, **17**(4), 06016030.

Vesga, L.F., Vallejo, L.E. and Lobo-Guerrero, S. (2008), "DEM analysis of the crack propagation in brittle clays under uniaxial compression tests", *Int. J. Numer. Anal. Meth. Geomech.*, **32**(11), 1405-1415.

Wang, Z., Ruiken, A., Jacobs, F. and Ziegler, M. (2014), "A new suggestion for determining 2D porosities in DEM studies", *Geomech. Eng.*, **7**(6), 665-678.

Wu, S. and Xu, X. (2016), "A study of three intrinsic problems of the classic discrete element method using flat-joint model", *Rock Mech. Rock Eng.*, **49**(5), 1813-1830.

Xu, W.J., Li, C.Q. and Zhang, H.Y. (2015), "DEM analyses of the mechanical behavior of soil and soil-rock mixture via the 3D direct shear test", *Geomech. Eng.*, **9**(6), 815-827.

Xue, X. (2015), "Study on relations between porosity and damage in fractured rock mass", *Geomech. Eng.*, **9**(1), 15-24.

Yang, B., Jiao, Y. and Lei, S. (2006), "A study on the effects of microparameters on macroproperties for specimens created by bonded particles", *Eng. Comput.*, **23**(6), 607-631.

Yoon, J. (2007), "Application of experimental design and optimization to PFC model calibration in uniaxial compression simulation", *Int. J. Rock Mech. Min. Sci.*, **44**(6), 871-889.

Zhao, W., Huang, R. and Yan, M. (2015), "Mechanical and fracture behavior of rock mass with parallel concentrated joints with different dip angle and number based on PFC simulation", *Geomech. Eng.*, **8**(6), 757-767.

Zhou, L., Chu, X., Zhang, X. and Xu, Y. (2016), "Numerical investigations on breakage behaviour of granular materials under triaxial stresses", *Geomech. Eng.*, **11**(5), 639-655.

CC